IEEE Access
Multidisciplinary | Rapid Review | Open Access Journal

Received January 28, 2020, accepted February 14, 2020, date of publication February 21, 2020, date of current version March 3, 2020.

Digital Object Identifier 10.1109/ACCESS.2020.2975597

Power Transfer by Volume Conduction: In Vitro Validated Analytical Models Predict DC Powers Above 1 mW in Injectable Implants

MARC TUDELA-PI[1], LAURA BECERRA-FAJARDO[1], ARACELYS GARCÍA-MORENO[1], JESUS MINGUILLON[1], AND ANTONI IVORRA[1,2]

[1]Department of Information and Communications Technologies, Universitat Pompeu Fabra, 08018 Barcelona, Spain
[2]Serra Húnter Fellow Programme, Universitat Pompeu Fabra, 08018 Barcelona, Spain

Corresponding author: Antoni Ivorra (antoni.ivorra@upf.edu)

This work was supported by the European Research Council (ERC) under the European Union's Horizon 2020 Research and Innovation Programme under Grant 724244. The work of Antoni Ivorra was supported by the ICREA under the ICREA Academia Programme.

ABSTRACT Galvanic coupling, or more precisely volume conduction, has been recently studied by different research groups as a method for intrabody communications. However, only in a very few occasions its use for powering implants has been proposed and proper analyses of such capability are still lacking. We present the development and the *in vitro* validation of a set of analytical expressions able to estimate the maximum ac and dc powers attainable in elongated implants powered by volume conduction. In particular, the expressions do not describe the complete power transfer channel but the behavior of the implants when the presence of an electric field is assumed. The expressions and the *in vitro* models indicate that time-averaged powers above 1 mW can be readily obtained in very thin (diameter < 1 mm) and short (length < 15 mm) implants when ac fields that comply with safety standards are present in the tissues where the implants are located. The expressions and the *in vitro* models also indicate that the obtained dc power is maximized by delivering the ac field in the form of short bursts rather than continuously. The study results support the use of volume conduction as a safe option to power implants.

INDEX TERMS Conducting materials, implantable biomedical devices, implantable electrodes, wireless power transmission.

I. INTRODUCTION[1]

In the field of active implantable medical devices (AIMDs), miniaturization is hampered because of the use of batteries and inductive coupling as energy sources [1]–[4]. Modern battery technologies offer too low energy densities for sub-millimetric miniaturization [5] and power transfer by inductive coupling, although it offers the additional benefit of allowing communications [6]–[11], requires embedding wide and rigid coils within the implants.

Non-electrical power transfer methods, based on ultrasounds [12]–[16] or infrared light [17], [18], have been occasionally proposed and demonstrated as alternatives to inductive coupling for transmitting power to AIMDs [19]. In addition, research efforts are being carried out for developing the so-called energy harvesters, also known as energy scavengers, which may provide electrical energy to AIMDs from energy sources available within the human body; typically from movements and temperature gradients [20], [21]. However, all these methods require bulky and rigid parts (e.g., piezoelectric crystals or photodiodes) within the implant that are typically much larger than the electronics they feed. To the best of our understanding, for power consumptions in the order of 1 mW, none of these methods is capable of allowing the development of AIMDs shaped as thin rods with diameters below 1 mm, which is a conformation highly beneficial in terms of minimal invasiveness as it allows percutaneous deployment (i.e., injection instead of surgery) [22]–[24].

We have recently shown *in vivo* that galvanic coupling, or more precisely volume conduction, can be an effective power transfer method for injectable AIMDs [25].

The associate editor coordinating the review of this manuscript and approving it for publication was Masood Ur-Rehman.

[1]A small portion of this study (the analysis on absolute maximum attainable power) was presented in a conference paper [48].

Remarkably, although galvanic coupling for intrabody communications has been studied lately by different research groups [26], it appears that recently only in a very few occasions, besides in our own publications, its use for powering implants has been explicitly proposed [27]–[29]. It must be noted, however, that in a few additional studies power transfer by volume conduction is also proposed but referred to as capacitive coupling [30]–[32].

To the best of our knowledge, we are pioneering the development of thread-like implants to be deployed deeply within tissues and to be powered by volume conduction. Other authors on power transfer by volume conduction have favored planar configurations to be deployed subcutaneously as these configurations obviously exhibit higher power transfer efficiency. However, we deem those planar configurations to be of little practical interest. They require much more complex implantation procedures than those required for tubular geometries which can be deployed by injection or catheterization [23], [33], [34].

The present study is intended to support the exploration of volume conduction as a power transfer method for allowing the development of very thin and flexible AIMDs suitable for deployment through injection or catheterization. We present the development, and the *in vitro* validation, of a set of analytical expressions able to estimate the maximum ac and dc powers attainable in elongated AIMDs which are powered by volume conduction. In particular, the expressions estimate the maximum ac and dc powers that the implants can obtain (or ''harvest'') when ac fields that comply with safety standards are present in the tissues where the implants are located.

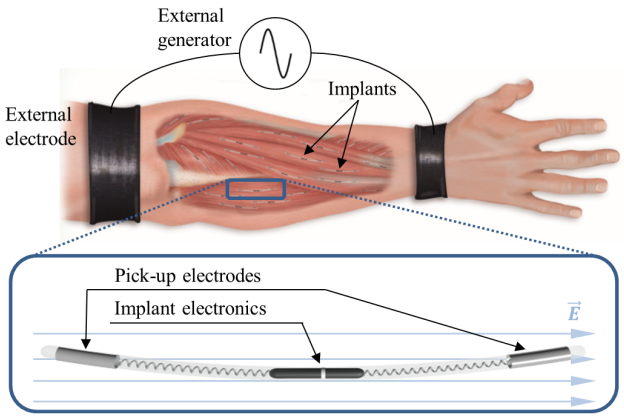

FIGURE 1. Hypothetical scenario of use for the proposed power transfer method. An ac electric field is generated in the forearm tissues across a pair of external electrodes. The implants draw electrical power using two electrodes located at their opposite ends. The devices could be used, for instance, as electrical stimulators or sensors.

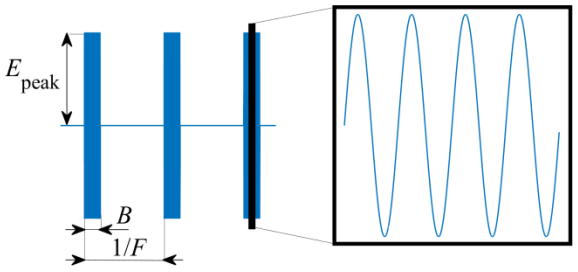

FIGURE 2. The delivered electric field consists in a sinusoidal waveform of frequency f and amplitude E_{peak} that can be applied continuously or in the form of bursts with duration B and repetition frequency F.

II. METHODS: MODELS

A. GENERAL FEATURES OF THE MODELS

The expressions developed in this study model the presence of an elongated implant within a tissue where an electric field exists due to external delivery of current. The modeled implant consists of two pick-up electrodes at its opposite ends and an electrical load (i.e., the electronics to be powered). This setup would represent hypothetical scenarios of use for the proposed power transfer method such as the scenario depicted in Fig. 1.

The electric field is modeled as homogeneous at the location of the implant and it consists in a sinusoidal waveform of frequency f and amplitude E_{peak} that can be applied continuously or in the form of bursts with duration B and repetition frequency F (Fig. 2). Unless otherwise stated, $f = 5$ MHz. The angle formed by the field and the implant (i.e., direction defined by the two electrodes of the implant) is α. Unless otherwise stated, $\alpha = 0$.

In order to develop concise analytical expressions, the following assumptions and simplifications were made (most of them illustrated in Fig. 3):

1) The implant is modeled as two conductive spheres, representing its pick-up electrodes (diameter D and inter-center separation L) and a resistance R_{Load} across these two electrodes that accounts for the electronics of the device (Fig. 3a).
2) The volume of homogeneous medium surrounding the implant is infinite relative to the dimensions of the implant.
3) The medium surrounding the implant (i.e. body tissue) is resistive. That is, rather than modeling the tissue surrounding the implant with, for instance, a Cole impedance model as it would be appropriate in a multi-frequency study, the tissue is modeled with a single resistance. This assumption is supported by the fact that at a single sinusoidal frequency the passive electrical properties of any material are appropriately modeled by a RC circuit (see Fig. 3b) and, at the frequencies considered here (1 MHz $< f <$ 20 MHz), soft tissues are predominately resistive and the capacitive component can be neglected [35]. In particular, the phase of the admittivity of muscle tissue is only 11.5° at 1 MHz, 8.7° at 10 MHz and 10.8° at 20 MHz [36].
4) The passive electrical properties of the medium (i.e., body tissue) surrounding the implant are isotropic. This assumption is supported by the fact that when high-frequency current is applied through the tissues,

the capacitive membranes of the cells are virtually short-circuited, thus making the tissue isotropic [37]. Even in the case of muscle tissue, which is highly anisotropic at low frequencies, it can be considered isotropic for frequencies above 1 MHz [38].

5) The skin effect is considered negligible. The skin effect causes ac current density to concentrate near the surface of the conductors and hinders electric field penetration. However, in human tissues, because their relatively poor conductivity, the skin effect only becomes significant at frequencies well above 10 MHz [40]. As latter discussed, for power transfer by volume conduction, we recommend the use of field frequencies below 20 MHz because of the skin effect.
6) The electrode-electrolyte interface impedance is considered negligible. This assumption is supported by the fact that the interface impedance of metal electrodes is roughly equivalent to a capacitance above 0.1 F/m^2 [39] that, for the electrode dimensions and the frequencies considered here, translates into an impedance magnitude in the order of tenths of ohm or a few ohms (e.g., 0.4 Ω for a spherical electrode with a diameter D of 0.5 mm and at a frequency f of 5 MHz). Therefore, the electrode-electrolyte impedance is negligible to the equivalent resistance across the implant electrodes (see Section II.C).

B. LIMITATIONS IMPOSED BY SAFETY STANDARDS

The safety standards developed by IEEE [41] and the International Commission on Non-Ionizing Radiation Protection (ICNIRP) [42], [43] implicitly limit the maximum value of E_{peak}. These safety standards for human exposure to electromagnetic fields identify two general sources of risk regarding passage of radiofrequency (RF) currents through the body: 1) risk of thermal damage due to the Joule heating and 2) risks caused by unsought electrical stimulation of excitatory tissues with harmful effects ranging from mild perception to death by ventricular fibrillation.

The limitations specified by the standards regarding heating are indicated as a limitation to the so-called Specific Absorption Rate (*SAR*). It can be calculated at any point of the tissue with the following expression

$$SAR = \frac{\sigma\,(E_{\text{rms}})^2}{\rho} \tag{1}$$

where σ is the electrical conductivity of the tissue (S/m), ρ is the mass density of the tissue (kg/m^3) and E_{rms} is the root mean square value of the electric field in the tissue (V/m).

Both the IEEE standard and the ICNIRP guidelines indicate the same *SAR* limitations averaged over 6 minutes and 10 g mass of tissue for localized exposure in the frequency range from 100 kHz to 3 GHz. For general public and at any human body location the *SAR* limit is 2 W/kg. For occupational exposure or persons in controlled environments – as would be the case considered here – this limit is 10 W/kg and it is further increased up to 20 W/kg if the localized exposure is at extremities. The *SAR* limit entails the following limitation for continuous sinusoidal fields

$$E_{\text{peak}} \leq \sqrt{\frac{2\rho SAR}{\sigma}} \tag{2}$$

and for fields applied in the form of sinusoidal bursts

$$E_{\text{peak}} \leq \sqrt{\frac{2\rho SAR}{\sigma FB}}. \tag{3}$$

Unless otherwise stated, here the *SAR* limit of 10 W/kg averaged over 10 g of tissue has been considered. At 5 MHz and in muscle tissue ($\sigma = 0.59$ S/m [36], $\rho \approx 1000$ kg/m^3 [44]), this field amplitude limit is roughly 180 V/m for $FB = 1$ and 580 V/m for $FB = 0.1$.

The standards indicate that above a specified frequency the risks caused by unsought electrical stimulation are negligible and only the *SAR* limitation applies. This frequency is 5 MHz in the case of the IEEE standard, which we deem more precisely defined than the ICNIRP standard regarding the specification of the limits to avoid the risks of unsought stimulation. This eliminates the risk of unsought electrical stimulation for continuous sinusoidal fields. However, for sinusoidal fields applied in the form of bursts, the IEEE standard rightfully indicates that the low frequency harmonics must be checked and it specifies

$$\sum_{0}^{5\text{MHz}} \frac{E_n}{MPE_n} \leq 1 \tag{4}$$

where E_n is the magnitude of the n$^{\text{th}}$ Fourier component of the exposure E, and MPE_n is the maximum permissible exposure for n frequency. For persons in controlled environments and exposed tissues that are neither the brain nor the heart, the standard determines a *MPE* of $2.1\sqrt{2}$ V/m for frequencies below 3350 Hz. For frequencies above, the *MPE* is calculated as

$$MPE_n = \frac{2.1\sqrt{2}}{3350} f_n. \tag{5}$$

This condition establishes another limit to E_{peak} that can be lower than the threshold specified by the *SAR* limitation (3) for low duty cycles (see appendix A). For muscle tissue at 5 MHz ($\sigma = 0.59$ S/m [36]), if $FB \geq 0.1$ then this second threshold is higher than that imposed by the *SAR* limitation and hence it can be neglected.

C. ABSOLUTE MAXIMUM ATTAINABLE POWER

The implant is seen as a load by the tissues surrounding it. Therefore, since the passive electrical properties of tissues are linear, a Thévenin equivalent circuit can be implemented (Fig. 3b).

This Thévenin model (circuit outside dashed square/box in Fig. 3b composed of $v_{\text{Th}}(t)$ and R_{Th}) locally models the tissues surrounding the implant, the implant electrodes and the presence of the electric field.

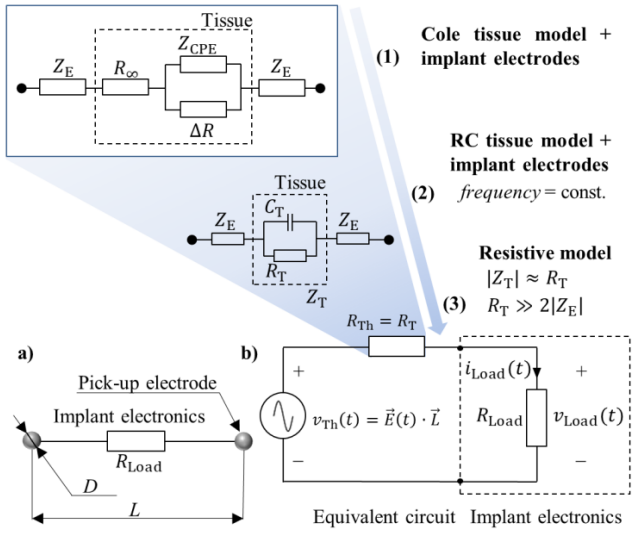

FIGURE 3. a) The implant is modeled as two conductive spheres, representing its pick-up electrodes, and a resistance across these two electrodes that accounts for the electronics of the device. b) The tissue surrounding the implant, the implant electrodes and the presence of an electric field are modeled with a Thévenin equivalent circuit. To obtain closed analytical expressions, the combined impedance of the tissue and the electrodes is simply modeled with a resistance (see II.A). This approximation can be understood as a three-step process: first, the accepted Cole impedance model for living tissues is simplified to an RC circuit considering that the frequency of the field is constant. Second, as stated in the text, because of the high operating frequencies, the tissue is considered predominantly resistive and C_T is neglected. Third, since the impedance of the electrodes is much smaller than the impedance across them, the impedance of the electrodes is neglected.

The Thévenin voltage is the open-circuit voltage. That is, the voltage across the implant electrodes when $R_{\text{Load}} = \infty$. If the electric field present at the location of the implant is sinusoidal, the Thévenin voltage ($v_{\text{Th}}(t)$) is also sinusoidal with amplitude [45]

$$V_{\text{Th peak}} = E_{\text{peak}} L \cos(\alpha) \tag{6}$$

or, in general, for any field waveform

$$V_{\text{Th rms}} = E_{\text{rms}} L \cos(\alpha). \tag{7}$$

The power drawn by the load is

$$P_{\text{Load}} = \frac{V_{\text{Load}}^2}{R_{\text{Load}}} = \frac{\left(V_{\text{Th rms}} \frac{R_{\text{Load}}}{R_{\text{Load}}+R_{\text{Th}}}\right)^2}{R_{\text{Load}}}. \tag{8}$$

For the circuit described in Fig. 3b, P_{Load} is maximized when R_{Load} matches R_{Th}. Hence the maximum power that the implant can draw is

$$\max(P_{\text{Load}}) = P_{\text{Load}}\Big|_{R_{\text{Load}}=R_{\text{Th}}} = \frac{(\max(V_{\text{Th rms}}))^2}{4R_{\text{Th}}}$$

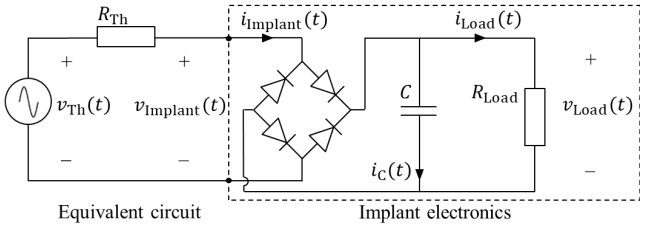

FIGURE 4. Basic circuit topology for extracting dc power, consisting of a diode bridge full-wave rectifier combined with a smoothing capacitor, connected to the Thévenin equivalent. The Thévenin equivalent models the tissue surrounding the implant and the presence of the electric field.

$$= \frac{(\max(E_{\text{rms}})\, L)^2}{4R_{\text{Th}}} = \frac{\max(SAR)\, \rho L^2}{4R_{\text{Th}}\sigma}. \tag{9}$$

The Thévenin resistance, R_{Th}, is the equivalent resistance across the implant electrodes as seen from the implant ($R_{\text{Load}} = \infty$). In an infinite volume, the resistance across two conductive spheres with a separation distance much larger than their diameter ($L \gg D$) can be approximated by [46]

$$R_{\text{Th}} = \frac{1}{\sigma \pi D}. \tag{10}$$

Hence the absolute maximum power that the implant can draw is

$$\max(P_{\text{Load}}) = \frac{\pi}{4} \max(SAR)\, \rho D L^2. \tag{11}$$

D. MAXIMUM UNREGULATED DC POWER

Most AIMDs will require dc power for functioning. In Fig. 4 it is represented the most likely circuit topology to be employed in AIMDs for extracting a dc power: a diode bridge full-wave rectifier combined with a smoothing capacitor.

For analyzing the behavior of this system, a procedure similar to that described in [47] is followed. Two assumptions are made. First, it is assumed that the ripple factor of the rectifier is almost zero. That is, the load voltage, $v_{\text{Load}}(t)$, is assumed to be constant (i.e., $v_{\text{Load}}(t) = V_{\text{Load}}$) once the circuit has reached steady-state.

Second, the diodes of the full-wave rectifier are modeled by the series combination of an ideal diode, an ideal voltage source (V_{Diode}) which accounts for the forward voltage and a resistance (R_{Diode}). Initially, it is also assumed that the electric field at the location of the implant is a continuous sinusoidal field.

Fig. 5 illustrates the main waveforms of the circuit under the previous assumptions.

The constant load voltage, V_{Load}, can be expressed as being equal to the value of the Thévenin voltage at specific time points

$$V_{\text{Load}} = |v_{\text{Th}}(kT_{\text{r}} \pm t_1)| = \left|V_{\text{Th peak}} \cos(kT_{\text{r}}\omega \pm \varphi)\right| \tag{12}$$

where k is an integer, T_r is the period of the rectified signal, ω is the angular frequency of the field and φ is a phase angle

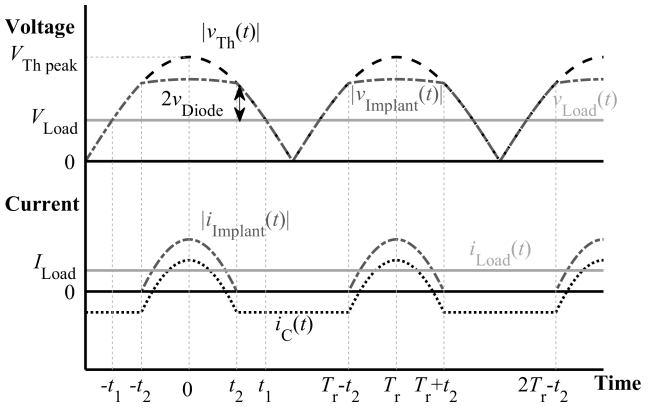

FIGURE 5. Schematic representation of the main waveforms of the circuit represented in Fig. 4.

that relates both voltages. In particular, for $k = 0$

$$V_{\text{Load}} = V_{\text{Th peak}} \cos(\varphi). \tag{13}$$

On the other hand, $i_{\text{Load}}(t)$ can be expressed as

$$i_{\text{Load}}(t) = \left|i_{\text{Implant}}(t)\right| - i_{\text{C}}(t). \tag{14}$$

Since $v_{\text{Load}}(t)$ is constant, $i_{\text{Load}}(t)$ is also constant

$$\begin{aligned} I_{\text{Load}} &= \frac{1}{T_r}\int_0^{T_r} i_{\text{Load}}(t)\,dt \\ &= \frac{1}{T_r}\int_0^{T_r} \left|i_{\text{Implant}}(t)\right| - i_{\text{C}}(t)\,dt. \end{aligned} \tag{15}$$

And since the average of $i_{\text{C}}(t)$ must be zero

$$I_{\text{Load}} = \frac{1}{T_r}\int_0^{T_r} \left|i_{\text{Implant}}(t)\right| dt. \tag{16}$$

The diode bridge only conduces when $|v_{\text{Th}}(t)| > v_{\text{Load}}(t) + 2V_{\text{Diode}}$. Therefore (17), as shown at the bottom of this page.

As indicated in Fig. 5, i_{Implant} flows between $kT_r - t_2$ and $kT_r + t_2$. These time points can be related to the phase of $v_{\text{Th}}(t)$ defining a new phase angle

$$\theta = \omega_r t_2 = \cos^{-1}\left(\frac{V_{\text{Load}} + 2V_{\text{Diode}}}{V_{\text{Th peak}}}\right). \tag{18}$$

Then I_{Load} can be calculated using (16) and (17) as follows

$$\begin{aligned} I_{\text{Load}} &= \frac{1}{T_r}\left[\int_0^{t_2} \frac{V_{\text{Th peak}}(\cos\omega t - \cos\varphi) - 2V_{\text{Diode}}}{2R_{\text{Diode}} + R_{\text{Th}}} dt \right. \\ &\quad \left. + \int_{T_r - t_2}^{T_r} \frac{V_{\text{Th peak}}(\cos\omega t - \cos\varphi) - 2V_{\text{Diode}}}{2R_{\text{Diode}} + R_{\text{Th}}} dt\right] \\ &= \frac{2}{\pi}\frac{V_{\text{Th peak}}\sin\theta - \theta\,(V_{\text{Load}} + 2V_{\text{Diode}})}{2R_{\text{Diode}} + R_{\text{Th}}}. \end{aligned} \tag{19}$$

From (13) and (19), the power obtained at the load is

$$\begin{aligned} P_{\text{Load dc}} &= V_{\text{Load}} I_{\text{Load}} \\ &= \frac{2V_{\text{Th peak}}}{\pi\,(2R_{\text{Diode}} + R_{\text{Th}})}\cos\varphi \\ &\quad \cdot\left[V_{\text{Th peak}}\sin\theta - \theta\,(V_{\text{Load}} + 2V_{\text{Diode}})\right]. \end{aligned} \tag{20}$$

It can be numerically verified that for a given $V_{\text{Th peak}}$ and a given V_{Diode} there is an optimum value of V_{Load} that maximizes the obtained dc power.

The absolute maximum possible dc power will be obtained in the case of no loses, that is, in the case of ideal diodes (i.e., $V_{\text{Diode}} = 0$ and $R_{\text{Diode}} = 0$). In this case (18) can be rearranged as

$$V_{\text{Load}} = V_{\text{Th peak}}\cos(\theta). \tag{21}$$

Comparing (13) with (21), we can assert that, for this case, θ is equal to φ. Thus (20) becomes

$$P_{\text{Load dc ideal}} = \frac{2V_{\text{Th peak}}^2}{\pi R_{\text{Th}}}\cos\varphi\,(\sin\varphi - \varphi\cos\varphi). \tag{22}$$

And it can be numerically determined that $P_{\text{Load dc ideal}}$ is maximum when $\varphi \approx 1.166 = \varphi_{\text{opt}}$ ($V_{\text{Load}} \approx 0.394\,V_{\text{Th peak}}$ and $R_{\text{Load}} \approx 1.35R_{\text{Th}}$).

Substituting (6) into (22), and noticing that E_{peak} has to fulfill (2), the maximum dc power that the implant can draw is

$$\begin{aligned} &\max(P_{\text{Load dc ideal}}) \\ &= \frac{4\max(SAR)\,\rho L^2}{\pi R_{\text{Th}}\sigma}\cos\varphi_{\text{opt}}\left(\sin\varphi_{\text{opt}} - \varphi_{\text{opt}}\cos\varphi_{\text{opt}}\right). \end{aligned} \tag{23}$$

For conductive spherical electrodes R_{Th} is calculated as (10), and in this case (23) becomes

$$\begin{aligned} &\max(P_{\text{Load dc ideal}}) \\ &= 4\max(SAR)\,\rho D L^2\cos\varphi_{\text{opt}}\left(\sin\varphi_{\text{opt}} - \varphi_{\text{opt}}\cos\varphi_{\text{opt}}\right). \end{aligned} \tag{24}$$

The ratio between the maximum dc power that the implants can draw (24) and the absolute maximum attainable power (11) is

$$\begin{aligned} \eta &= \frac{\max(P_{\text{Load dc ideal}})}{\max(P_{\text{Load}})} \\ &= \frac{16}{\pi}\cos\varphi_{\text{opt}}\left(\sin\varphi_{\text{opt}} - \varphi_{\text{opt}}\cos\varphi_{\text{opt}}\right) \\ &\approx 0.9226. \end{aligned} \tag{25}$$

The above expressions were found under the assumption of a continuous sinusoidal field. For fields in the form of

$$\left|i_{\text{Implant}}(t)\right| = \begin{cases} \dfrac{V_{\text{Th peak}}(\cos\omega t - \cos\varphi) - 2V_{\text{Diode}}}{R_{\text{Th}} + 2R_{\text{Diode}}}, & |v_{\text{Th}}(t)| > v_{\text{Load}}(t) + 2V_{\text{Diode}} \\ 0, & |v_{\text{Th}}(t)| \le v_{\text{Load}}(t) + 2V_{\text{Diode}} \end{cases} \tag{17}$$

sinusoidal bursts with duration B and repetition frequency F,

$$I_{\text{Load FB}} = \frac{2FB}{\pi} \frac{V_{\text{Th peak}} \sin\theta - \theta\,(V_{\text{Load}} + 2V_{\text{Diode}})}{2R_{\text{Diode}} + R_{\text{Th}}} \quad (26)$$

where the product FB is the duty cycle of the bursts and it is comprised between FB_{min} and 1, where FB_{min} is the minimum duty cycle to prevent unsought stimulation.

Hence the obtained power is

$$\begin{aligned} P_{\text{Load dc FB}} &= V_{\text{Load}} I_{\text{Load FB}} \\ &= \frac{2FBV_{\text{Th peak}}}{\pi\,(2R_{\text{Diode}} + R_{Th})} \cos\varphi \\ &\quad \cdot \left[V_{\text{Th peak}} \sin\theta - \theta\,(V_{\text{Load}} + 2V_{\text{Diode}})\right]. \end{aligned} \quad (27)$$

If $V_{\text{Th peak}} \gg 2V_{\text{Diode}}$ the phase angle θ defined in (18) will be equal to φ, see (13). Therefore, replacing θ by φ, and substituting (13) into (27) lead to

$$\begin{aligned} &P_{\text{Load dc FB}} \left(V_{\text{Th peak}} \gg 2V_{\text{Diode}}\right) \\ &\quad = \frac{2FBV_{\text{Th peak}}}{\pi\,(2R_{\text{Diode}} + R_{\text{Th}})} \cos\varphi\,[\sin\varphi - \varphi\cos\varphi]. \end{aligned} \quad (28)$$

E. MAXIMUM VOLTAGE-REGULATED DC CURRENT

In most practical cases the dc voltage will have to be regulated at a specific magnitude (e.g., +3.3 V) for powering the circuitry of the AIMD. Although switching regulators may be an option, because of size limitations, low-dropout (LDO) linear regulators will probably be preferred.

The circuit in Fig. 6 represents such scenario. Linear regulators provide a regulated dc voltage at their output (V_{Load}) if the dc voltage at their input satisfies $V_{\text{Reg}} \geq V_{\text{Load}} + V_{\text{Drop}}$, where V_{Drop} is the so-called dropout voltage, and they waste a small portion (I_{Q}) of the input current (I_{Reg}) so that $I_{\text{Load}} = I_{\text{Reg}} - I_{\text{Q}}$.

In this case, since V_{Load} is fixed, the objective is not to determine which is the maximum dc power at the load ($V_{\text{Load}}I_{\text{Load}}$) but the maximum current that can be obtained.

The load seen by the diode-bridge and the smoothing capacitor (C_1) is the combination of the actual load (R_{Load}) and the load of the LDO regulator. Hence the power expressions obtained above must be equaled to

$$\begin{aligned} P_{\text{Load+Reg}} &= V_{\text{Reg}} I_{\text{Reg}} \\ &= V_{\text{Reg}} \left(I_{\text{Load}} + I_{\text{Q}}\right). \end{aligned} \quad (29)$$

The maximum regulated dc current that can be obtained (I_{Load}) is that one that ensures that the regulator works properly, that is, that for $V_{\text{Reg}} = V_{\text{Load}} + V_{\text{Drop}}$.

III. METHODS: SETUP FOR IN VITRO VALIDATION OF THE MODELS

An *in vitro* experimental setup that replicates the assumptions made to develop the previous expressions was implemented (Fig. 7).

The ac electric field was delivered by two 86.5 mm×30 mm parallel aluminum plates acting as the external electrodes.

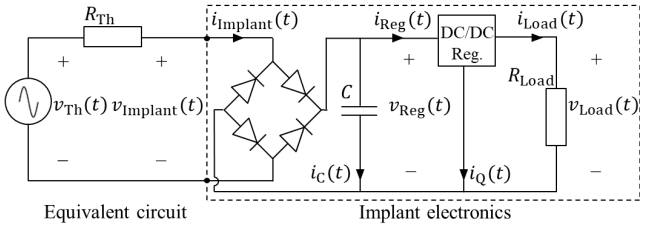

FIGURE 6. Basic circuit topology for obtaining a regulated dc voltage to power a load (R_{Load}). Here it is assumed that the DC/DC regulator consists of a linear regulator.

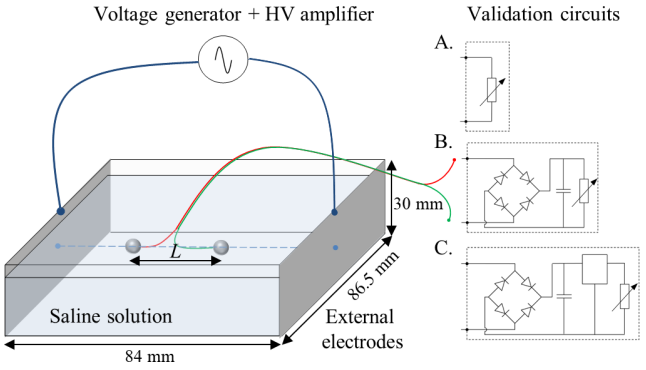

FIGURE 7. Schematic representation of the *in vitro* setup developed to validate the analytical models (see text for details).

These two electrodes were attached to opposite internal sides of a polycarbonate container (inner dimensions: 84 mm×86.5 mm×30 mm) filled with a NaCl solution whose conductivity was measured with a conductivity tester (HI 98312 by Hanna). Sinusoidal voltages, either continuous or in the form of bursts, were generated across the electrodes by the combination of a function generator (4064 by BK Precision) and a custom-made high-frequency (HF) high-voltage (HV) amplifier.

In all instances, the applied voltage was measured using a digital oscilloscope (TPS2014 by Tektronix). Unless otherwise stated, the amplitude of the applied voltage (A) was adjusted to obtain a *SAR* of 10 W/kg (in particular, for the described experimental setup, this corresponds to 2.2 W). That is,

$$A = \sqrt{\frac{2\rho SAR}{\sigma FB}}\, d \quad (30)$$

where d is the distance between the plate electrodes (84 mm).

The dimensions of this setup were chosen to be large for maximizing the uniformity of the electric field at the location of the pick-up electrodes while allowing the use of the custom-made high-frequency high-voltage amplifier (limited to 180 V, 1 A and 5 MHz).

The pick-up electrodes of the implants were represented by stainless steel (SAE 317) spherical electrodes with three different diameters: 0.5 mm, 1 mm, and 1.5 mm. Each electrode was laser welded to a 5 cm piece of 32 AWG enameled copper

wire. The ends of the copper wires were connected to the validation circuits described below.

A. VALIDATION CIRCUIT FOR ABSOLUTE MAXIMUM ATTAINABLE POWER

To validate (11), the pick-up electrodes were connected to a high-precision potentiometer acting as a variable resistor (see validation circuit A. in Fig. 7). Before connection, the resistance of the potentiometer (R_{Load}) was adjusted to match R_{Th} as provided by (10). Such adjustment was performed using a multimeter (38XR-A by Amprobe). After connection, the load voltage, $v_{\text{Load}}(t)$, was recorded using the digital oscilloscope and max (P_{Load}) was calculated as the square of the rms recorded voltage divided by the value of R_{Load}, considering a time interval of 5 μs.

B. VALIDATION CIRCUIT FOR MAXIMUM UNREGULATED DC POWER

To validate (20) and (27), it was implemented a PCB with the implant circuit represented in Fig. 4. The diodes of the diode-bridge were Schottky diodes (RB521ZS-30 by Rohm Semiconductor). The capacitor C had a capacitance of 10 μF. R_{Load} was again a high-precision potentiometer acting as a variable resistor.

The diode model parameters used in the analytical expressions were: $V_{\text{Diode}} = 0.2$ V and $R_{\text{Diode}} = 14\ \Omega$.

In the experiments reported below in which the value of R_{Load} was not fixed, the expression for P_{Loaddc} was numerically maximized for obtaining the optimum φ value and hence the optimum R_{Load} was found for maximum power. When the value of R_{Load} was fixed, the expression for $P_{\text{Load dc FB}}$ was numerically maximized for obtaining the optimum FB value.

C. VALIDATION CIRCUIT FOR MAXIMUM VOLTAGE-REGULATED DC CURRENT

A LDO regulator (ADP7112 by Analog Devices) adjusted to produce +3.3 V was mounted on the referred PCB to implement the implant circuit in Fig. 6. To study its analytical behavior, its quiescent current (I_{Q}) was set to 80 μA and its dropout voltage (V_{Drop}) to 30 mV. Both values are given by the manufacturer for $I_{\text{Load}} = 10$ mA. The capacitor C had a capacitance of 10 μF.

IV. RESULTS

A. DEPENDENCY ON INTER-ELECTRODE DISTANCE AND ON ELECTRODES DIAMETER

At $f = 5$ MHz, for a SAR of 10 W/kg and for the properties of a saline solution that resembles the properties of muscle tissue, Fig. 8 displays a set of results obtained by applying the analytical expressions together with the corresponding validation results using the *in vitro* setup. In particular, the absolute maximum attainable power, max (P_{Load}), in Fig. 8a, and the maximum obtained dc (unregulated) power, max (P_{LoadDC}) and max ($P_{\text{LoadDC FB}}$), in Fig. 8b and in Fig. 8c, are represented as a function of the inter-electrode distance (L) and the electrodes diameter (D). Besides confirming the validity of the models, these results indicate that dc powers above 1 mW can be obtained in very thin (diameter < 1 mm) and short (length < 15 mm) implants. Harvested dc power is larger when the sinusoidal electric field is delivered in the form of bursts (Fig. 8c), than when it is delivered continuously (Fig. 8b). However, even when the field is delivered in the form of bursts, the obtained dc power is still considerably smaller than the absolute maximum attainable power (Fig. 8a). This fall in performance becomes especially

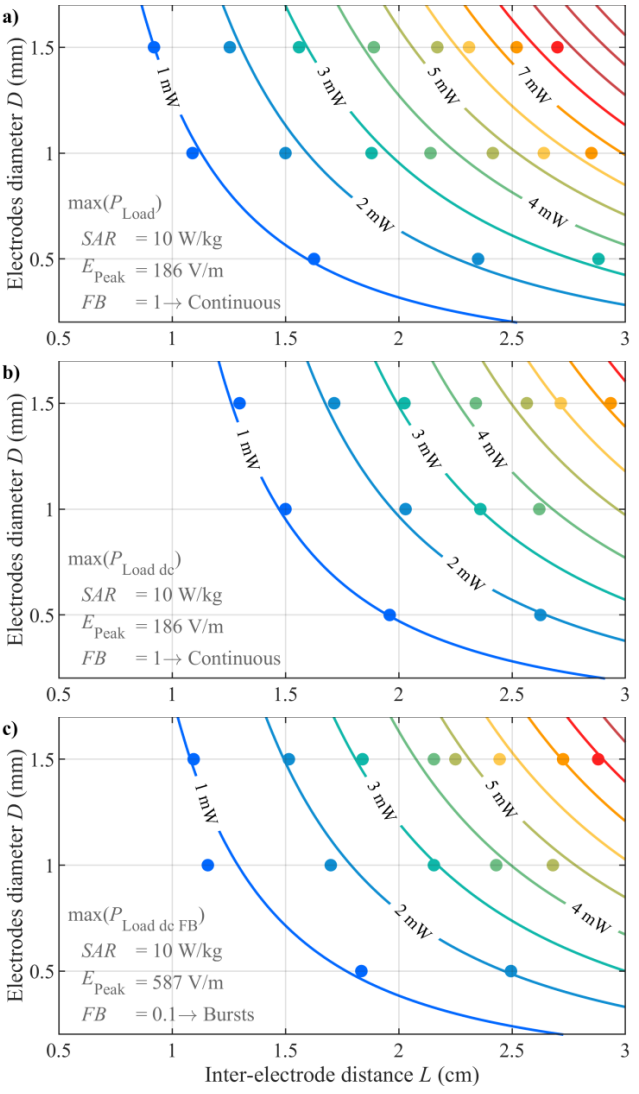

FIGURE 8. Dependency of the maximum power attainable at the implant load on the electrodes diameter (D) and on inter-electrode distance (L). Conditions: $SAR = 10$ W/kg, $f = 5$ MHz, $\sigma = 0.58$ S/m (0.3% NaCl) and $\rho = 1000$ kg/m^3. Solid lines: results from the analytical expressions; a) (11), b) (20), c) (27). Circles: experimental results; a) using Fig. 7.A, b) and c) the circuit represented in Fig. 4. a) Absolute maximum attainable power. b) maximum dc (unregulated) attainable power for a continuous sinusoidal field. c) maximum dc (unregulated) attainable power for a sinusoidal field applied in the form of bursts ($F = 10$ kHz, $B = 50$ μs).

noticeable for short inter-electrode distances. As further stressed in the following sub-sections, fall in performance is more severe for short implants because the voltage picked up by the implant electrodes approaches the magnitude of the forward voltage of the rectifier diodes and hence the relative energy losses are higher.

B. DEPENDENCY ON THE CONDUCTIVITY OF THE MEDIUM

As (11) indicates, and as we *in vitro* demonstrated in [48], the absolute maximum attainable power is independent of the conductivity of the medium.

Therefore, here only the dependency of max (P_{LoadDC}) on the conductivity of the medium is inspected. In Fig. 9, harvested dc power is surveyed for three different NaCl solutions with conductivities representative of those found in human tissues. In the case of a continuous field (Fig. 9a) it can be observed a notable dependency on the conductivity of the medium.

For instance, for $L = 3$ cm, the obtained dc power for $\sigma = 0.2$ S/m nearly doubles that for $\sigma = 1.52$ S/m. The main reason for this dependency is that E_{peak}, and hence V_{Thpeak}, must be reduced at higher conductivities for keeping the *SAR* value (2) and that causes bigger relative losses at the diodes of the full-wave rectifier.

On the other hand, if the field is applied in the form of bursts (Fig. 9b), since E_{peak}, and hence V_{Thpeak}, can be higher for the same *SAR*, the obtained dc power is not only higher but also less dependent on the conductivity of the medium. For instance, for $L = 3$ cm, the dc power for $\sigma = 0.2$ S/m is only about 20% higher than that for $\sigma = 1.52$ S/m.

C. DEPENDENCY ON LOAD RESISTANCE AND IMPEDANCE MATCHING

In the two previous sub-sections it was applied the optimum R_{Load} to maximize the harvested power. Since, in most scenarios, R_{Load} will be a non-adjustable parameter, it is worth inspecting how the harvested power depends on it.

In Fig. 10 it is displayed the dependency of the maximum attainable power on the value of R_{Load} for the range from 200 Ω to 200 kΩ in the case of a modeled implant with $D = 1$ mm and $L = 30$ mm in a medium with $\sigma = 0.58$ S/m. For these parameters $R_{\text{Th}} \approx 550$ Ω. If the voltage is not rectified, that is, if the resistive load is directly connected to the implant electrodes, the dissipated power at the load ($P_{\text{Load ac}}$) is maximum when $R_{\text{Load}} = R_{\text{Th}}$. That is the point at which the absolute maximum attainable power is reached. Similarly, a (lower) maximum harvested dc power is found at a $R_{\text{Load}} = R_{\text{Load Opt dc}}$ if the sinusoidal electric field is applied continuously.

In both cases the obtained power decreases substantially when R_{Load} is lower or higher than the optimum one. However, if the electric field is applied in the form of bursts, the drop in harvested dc power can be mitigated, and actually reverted, for loads above $R_{\text{LoadOptdc}}$. The use of bursts introduces an additional parameter for allowing power optimization: the duty cycle, *FB*.

By reducing *FB* the loss in performance due to the increase of R_{Load} can be compensated. Moreover, since by reducing *FB* the field amplitude, E_{peak}, can be increased for the same *SAR* value, the losses associated with the diodes are reduced and hence the power obtained at the load is higher

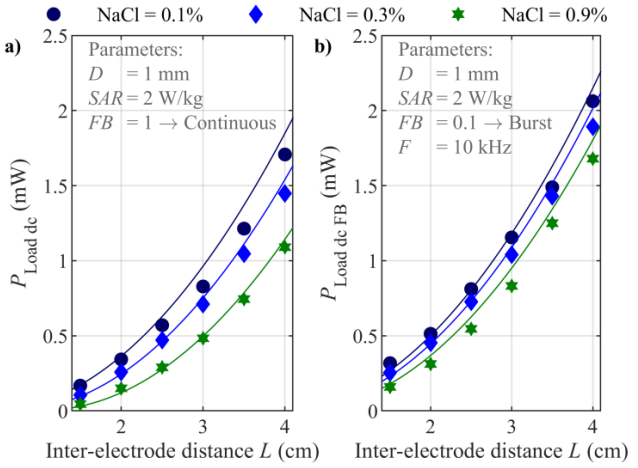

FIGURE 9. Dependency of the maximum dc power attainable at the implant load on the inter-electrode distance for three different conductivities of the medium. Conditions: $SAR = 2$ W/kg, $f = 5$ MHz, $\sigma_1 = 0.20$ S/m (0.1% NaCl), $\sigma_2 = 0.58$ S/m (0.3% NaCl), $\sigma_3 = 1.52$ S/m (0.9% NaCl), $\rho = 1000$ kg/m^3 and $D = 1$ mm. Solid lines: results from the analytical expressions; a) (20) and b) (27). Markings: experimental results using the circuit represented in Fig. 4. a) Maximum dc power when the field is applied continuously. b) Maximum dc power when the field is applied in the form of bursts ($F = 10$ kHz, $B = 10$ μs).

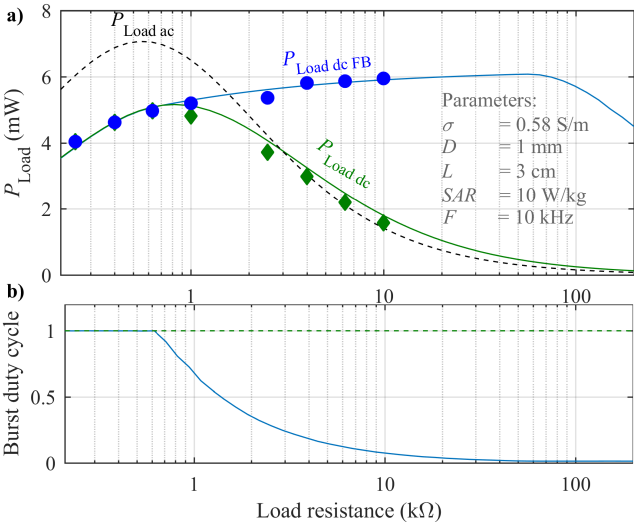

FIGURE 10. a) Dependency of the maximum dc power attainable at the implant load on the value of R_{Load}. Conditions: $SAR = 10$ W/kg, $f = 5$ MHz, $\sigma = 0.58$ S/m (0.3% NaCl), $\rho = 1000$ kg/m^3, $L = 3$ cm and $D = 1$ mm. Green trace and markings: maximum dc power for a continuous ac field (11). Blue trace and markings: maximum dc power for an ac field applied in the form of bursts (duty cycle optimized) (27). Solid lines: results from the analytical expressions. Markings: experimental results using the circuits represented in Fig. 4 (dc) and Fig. 7.A (ac). b) Optimum duty cycle, *FB*, for obtaining the results in subFig. a).

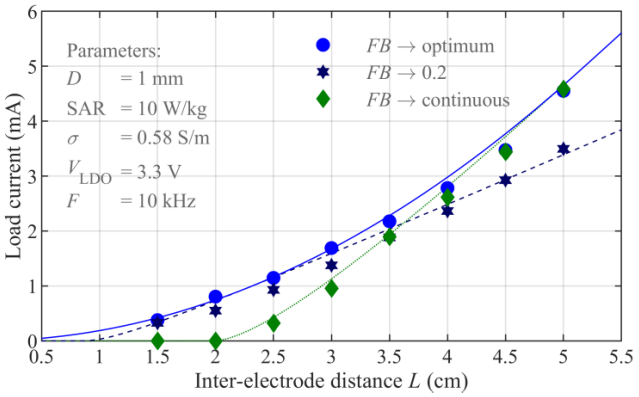

FIGURE 11. Dependency of the maximum voltage-regulated (+3.3 V) dc current attainable at the implant load on the inter-electrode distance (*FB*) for three different field patterns: continuous (green), in the form of bursts with a constant duty cycle of 0.2 (dark blue) and in bursts with an optimized duty cycle (blue). Conditions: $SAR = 10$ W/kg, $f = 5$ MHz, $\sigma = 0.58$ S/m (0.3% NaCl), $\rho = 1000$ kg/m^3 and $D = 1$ mm. Solid lines: results from the analytical expressions; continuous (19), bursts (26). Markings: experimental results; using the circuit represented in Fig. 6.

than that obtained for a continuous electric field at $R_{\text{Load}} = R_{\text{Load Opt dc}}$. As it can be observed in Fig 10, the obtained dc power reaches values ($\sim$ 6 mW) close to the absolute maximum attainable power ($\sim$ 7 mW). Nevertheless, *FB* cannot be reduced without limit.

As explained in Section II.B and in the appendix, *FB* must be limited to prevent unsought stimulation. In the case illustrated in Fig. 10, *FB* was limited accordingly and that causes the drop of power observable when R_{Load} is larger than 57 kΩ.

D. MAXIMUM VOLTAGE-REGULATED DC CURRENT

For a range of inter-electrode distances ($L \in$[0.5 cm, 5.5 cm]), Fig. 11 shows the maximum dc current attainable at the output of the linear regulator (Fig. 6) when the ac electric field is applied in three different ways: continuously, in bursts with a constant duty cycle ($FB = 0.2$) and in bursts with a duty cycle optimized for the load seen by the diode-bridge.

For short implants it can be clearly noticed the benefit of using ac fields in the form of bursts. If a continuous ac field is employed, voltage regulator operation is impossible for implants of 2 cm or shorter whereas, for that same length, if the field is applied in the form of bursts, operation is possible and currents of 500 μA can be readily drawn by the load.

In addition, the results displayed in Fig. 11 also illustrate the importance of optimizing the duty cycle: to obtain a current of 500 μA the minimum implant length is 1.65 cm in the case of optimum *FB* whereas such minimum length has to be increased to 2.56 cm if the constant duty cycle is used.

V. DISCUSSION

As stated in the introduction, only in a very few occasions the use of volume conduction for powering AIMDs has been proposed and studied. And, to the best of our knowledge, no commercial AIMDs use it. The reasons why other teams are reluctant – or did not conceive – to use volume conduction for power thin and elongated implants can only be guessed.

We conjecture that the reluctance mainly arises from not recognizing two facts about volume conduction. First, large magnitude high frequency (> 1MHz) currents can safely flow through the human body if applied as short bursts. Second, to obtain a sufficient voltage drop across its two intake (pick-up) electrodes, the implant can be shaped as a thin and flexible elongated body (Fig. 1) which is a configuration highly suitable for minimally invasive deployment through injection or catheterization.

One of the few studies in which volume conduction has been studied for powering elongated implantable devices is [29]. Although that study reinforces the main notion of the present study (i.e., volume conduction can be an effective method for powering AIMDs), it must be noted that some of the results and conclusions of that study are implausibly benign according to the assumptions and results of the present study. For instance, that study reports that with an inter-electrode distance of only 1 mm the implant can harvest a dc voltage of 0.44 V when the SAR is below 1 W/kg ($f = 13.9$ MHz, $FB = 1$). We deem this result is implausible because a harvested dc voltage of 0.44 V by an implant placed 5 cm inside the tissues would imply $V_{\text{Th}} \geq 0.44$ V which in turn would imply $E_{\text{Th}} \geq 440$ V/m in its surrounding tissues. Furthermore, since volume conduction is a non-focalized wireless power transfer method, the electric field is expected to be higher in more superficial locations. Although we do not have enough information to compute the exact value of the *SAR* averaged over 10 g of tissue, the magnitude of the electric field in the implant location together with the distance between external electrodes (from 2 to 5 cm), leads us to be skeptical about the feasibility of achieving the powers reported in [29] without exceeding the limits established by international safety standards. Another result of that study that we deem implausible is the absence of a significant impact on the obtained power by the relative angle between the external electrodes and the implant electrodes. Since the electric field direction depends on the orientation of the external electrodes, such result would imply that the obtained power is independent of α. And this, as illustrated in Fig. 12, is far from what our models and previous results [25] indicate: if the electric field is perpendicular to the implant then the harvested power is null.

Powering AIMDs by volume conduction requires the delivery of currents through external electrodes so that electric fields appear in the tissues where the AIMDs are located. For the sake of brevity and simplicity, the aspects related to current delivery are intentionally neglected in the present study; the presence of a homogeneous electric field is assumed. We will treat these aspects in subsequent studies. However, there is an aspect worth briefly discussing now: the impact of the skin effect. In particular, at 10 MHz the current density 10 cm deep within muscles, $J_{10\text{ cm}}$, is approximately half

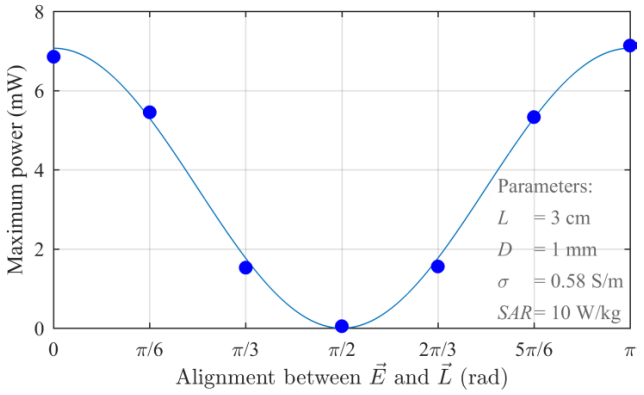

FIGURE 12. Dependency of the absolute maximum power attainable at the implant load on the angle (α) between the electric field and the implant. Conditions: $SAR = 10$ W/kg, $f = 5$ MHz, $FB = 1$, $L = 30$ mm, $D = 1$ mm, $\sigma = 0.58$ S/m (0.3% NaCl) and $\rho = 1000$ kg/m^3. Solid lines: results from the analytical model (11). Circles: experimental results (the two-spheres arrangement for the implant electrodes in Fig. 7 was rotated with respect to the plate electrodes) using the circuit represented in Fig. 7.A.

of the current density at the surface, J_0; and at 100 MHz $J_{10\text{cm}} = 0.1J_0$. Therefore, it appears sensible not to use frequencies significantly above 10 MHz if it is intended to power deep seated implants. That is why we recommend the use of frequencies below 20 MHz (but above 5 MHz to prevent unsought stimulation).

Another limitation of the present study is that, again for the sake of simplicity, the shape of the pick-up electrodes was restricted to spheres. This limits their surface area and hence hinders reducing R_{Th}. It is worth noting that, for a given electrode diameter (e.g., the maximum allowed by the lumen of a needle), larger powers than those reported here will be harvested if the electrodes are shaped as cylinders rather than as spheres since they will have a lower R_{Th} [46]. Recalling from (8), this will imply higher power harvested.

The results obtained here show minor differences between the model and the data obtained *in vitro*. These differences are most likely due to geometrical tolerances in the *in vitro* setup, and limitations in terms of resolution and accuracy imposed by the measurement equipment.

In terms of power transfer efficiency, the specificity of the setup used in this study limits the direct comparison of the results with those obtained with other wireless power transfer technologies such as inductive coupling and ultrasonic power transfer. Therefore, this comparison falls out of the scope of this paper. However, it is worth noting that we envision systems with the power transfer efficiencies (PTE) ranging from 0.01% to 1%. For instance, we performed a numerical study in which it was simulated power transfer by volume conduction to stimulation implants in an anatomically realistic leg model and we obtained a PTE of about 0.05% with an input power requirement of less than 4 W, which is low enough to grant the use of small portable rechargeable batteries [49]. Additionally, it must be noted that the results obtained here demonstrate that the maximum attainable power can be well above 1 mW and that such power is enough to supply the electronics of most AIMDs. For instance, power consumption of the electronics of a recently commercialized injectable glucose sensor (Eversense by Senseonics Inc.) is in the order of 250 μW [50].

VI. CONCLUSION

This study supports the use of volume conduction as a safe option to power very thin and flexible AIMDs. It provides a theoretical framework for optimizing both the design of the implants and the applied electric fields used to power them.

The developed analytical expressions, which are *in vitro* validated in the present study, indicate that dc powers above 1 mW can be readily obtained in very thin (diameter < 1 mm) and short (length < 15 mm) implants when ac electric fields that comply with safety standards are present in the tissues where the implants are located. Other main conclusions are:

1) The obtained dc power is maximized by delivering the ac field in the form of short bursts rather than continuously.
2) The maximum attainable dc power depends on the conductivity of the medium. Such dependency is minimized by delivering the ac field in the form of short bursts rather than continuously.
3) Both the absolute maximum attainable power and the maximum attainable dc power exhibit a distinctive maximum for a specific load resistance (i.e., optimum load resistance). If the ac field is delivered in the form of bursts rather than continuously, it is possible to set the value of the optimum load resistance by adjusting the duty cycle of the bursts.

The use of volume conduction for powering AIMDs could overcome some of the limitations imposed by other technologies in terms of size and invasiveness. This would improve the deployment and usability of AIMDs in several applications such as bioelectronic medicines [51], neuro-prostheses [52] and implantable sensors [53].

APPENDIX

Appendix A. Maximum field amplitude limited by unsought simulation in the case of sinusoidal electric fields applied in the form of bursts.

The waveform obtained for this case considering a single period can be mathematically expressed as

$$E(t) = \begin{cases} E_{\text{peak}} \sin(2\pi f t), & |t| < B/2 \\ 0, & |t| \geq B/2 \end{cases} \quad \text{(A.1)}$$

where E_{peak} must fulfill (3) to avoid tissue overheating. The complex Fourier series representation of (A.1) can be defined as

$$E(t) = \sum_{n=-\infty}^{\infty} c_n e^{in2\pi Ft}. \quad \text{(A.2)}$$

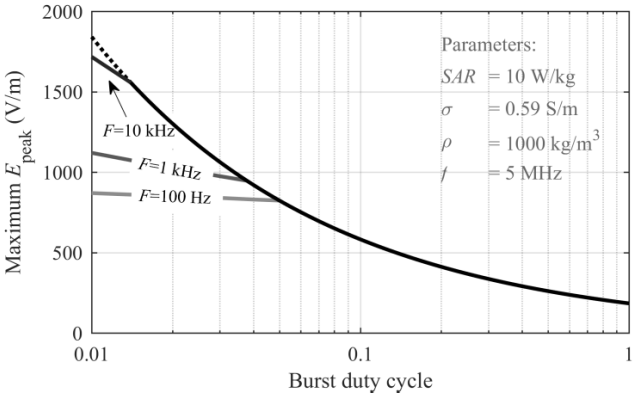

FIGURE 13. Maximum E_{peak} allowed for avoiding tissue overheating and stimulation. Solid lines: maximum E_{peak} for $F = 100$ Hz, $F = 1$ kHz, and $F = 10$ kHz. Dashed line: maximum E_{peak} due to the *SAR* restriction for F above 10 kHz. Conditions: $SAR = 10$ W/kg, $f = 5$ MHz, $\sigma = 0.59$ S/m, and $\rho = 1000$ kg/m^3.

The complex Fourier coefficients of (A.2) can be determined as

$$c_n = F \int_{-B/2}^{B/2} E(t)\, e^{-in2\pi Ft} \mathrm{d}t \tag{A.3}$$

Integrating (A.3) and applying

$$E_n = \begin{cases} \dfrac{E_{\text{peak}} FB}{2}, & Fn = f \\ 2|c_n|, & Fn \neq f \end{cases} \tag{A.4}$$

the E_n magnitude of the n^{th} Fourier component of the exposure field can be determined. Finally, the obtained set of E_n has to fulfill (4) to avoid possible stimulation. In this studied case, (4) limits the maximum E_{peak} when FB tends to be much lower than 1. This fact is illustrated in Fig. 13. Considering a $SAR = 10$ W/kg, $f = 5$ MHz, $\sigma = 0.59$ S/m, and $\rho = 1000$ kg/m^3 it can be noticed that for $FB > 0.05$ and $F > 100$ Hz the maximum E_{peak} is limited due to the *SAR* restriction (3). On the other hand, when FB is decreased (4) has to be considered. Remarkably, considering the same FB, for higher F, higher E_{peak} amplitudes can be safely applied.

REFERENCES

[1] M. Nathan, "Microbattery technologies for miniaturized implantable medical devices," *Current Pharmaceutical Biotechnol.*, vol. 11, no. 4, pp. 404–410, Jun. 2010.
[2] S. Rao and J. Chiao, "Body electric," *IEEE Microw. Mag.*, vol. 16, no. 2, pp. 54–64, 2015.
[3] A. Kiourti and K. S. Nikita, "A review of in-body biotelemetry devices: Implantables, ingestibles, and injectables," *IEEE Trans. Biomed. Eng.*, vol. 64, no. 7, pp. 1422–1430, Jul. 2017.
[4] H. Munaf, "Leadless pacemakers?: A new era in cardiac pacing," *J. Cardiol.*, vol. 67, no. 1, pp. 1–5, 2016.
[5] M. Rasouli and L. S. J. Phee, "Energy sources and their development for application in medical devices," *Expert Rev. Med. Devices*, vol. 7, no. 5, pp. 693–709, Jan. 2014.
[6] D. Guiraud, T. Stieglitz, G. Taroni, and J.-L. Divoux, "Original electronic design to perform epimysial and neural stimulation in paraplegia," *J. Neural Eng.*, vol. 3, no. 4, pp. 276–286, Sep. 2006.
[7] M. Ghovanloo and K. Najafi, "A wideband frequency-shift keying wireless link for inductively powered biomedical implants," *IEEE Trans. Circuits Syst. I, Reg. Papers*, vol. 51, no. 12, pp. 2374–2383, Dec. 2004.
[8] S. A. Mirbozorgi, P. Yeon, and M. Ghovanloo, "Robust wireless power transmission to mm-sized free-floating distributed implants," *IEEE Trans. Biomed. Circuits Syst.*, vol. 11, no. 3, pp. 692–702, Jun. 2017.
[9] D. Ahn and M. Ghovanloo, "Optimal design of wireless power transmission links for millimeter-sized biomedical implants," *IEEE Trans. Biomed. Circuits Syst.*, vol. 10, no. 1, pp. 125–137, Feb. 2016.
[10] N. Ha-Van and C. Seo, "Modeling and experimental validation of a butterfly-shaped wireless power transfer in biomedical implants," *IEEE Access*, vol. 7, pp. 107225–107233, 2019.
[11] H.-J. Kim, H. Hirayama, S. Kim, K. J. Han, R. Zhang, and J.-W. Choi, "Review of near-field wireless power and communication for biomedical applications," *IEEE Access*, vol. 5, pp. 21264–21285, 2017.
[12] M. Sahin and V. Pikov, "Wireless microstimulators for neural prosthetics," *Crit. Rev. Biomed. Eng.*, vol. 39, no. 1, pp. 63–77, 2011.
[13] D. Seo, J. M. Carmena, J. M. Rabaey, M. M. Maharbiz, and E. Alon, "Model validation of untethered, ultrasonic neural dust motes for cortical recording," *J. Neurosci. Methods*, vol. 244, pp. 114–122, Apr. 2015.
[14] A. Ibrahim, M. Meng, and M. Kiani, "A comprehensive comparative study on inductive and ultrasonic wireless power transmission to biomedical implants," *IEEE Sensors J.*, vol. 18, no. 9, pp. 3813–3826, May 2018.
[15] T. C. Chang, M. J. Weber, J. Charthad, S. Baltsavias, and A. Arbabian, "End-to-end design of efficient ultrasonic power links for scaling towards submillimeter implantable receivers," *IEEE Trans. Biomed. Circuits Syst.*, vol. 12, no. 5, pp. 1100–1111, Oct. 2018.
[16] R. V. Taalla, M. S. Arefin, A. Kaynak, and A. Z. Kouzani, "A review on miniaturized ultrasonic wireless power transfer to implantable medical devices," *IEEE Access*, vol. 7, pp. 2092–2106, 2019.
[17] K. Mathieson, J. Loudin, G. Goetz, P. Huie, L. Wang, T. I. Kamins, L. Galambos, R. Smith, J. S. Harris, A. Sher, and D. Palanker, "Photovoltaic retinal prosthesis with high pixel density," *Nature Photon.*, vol. 6, no. 6, pp. 391–397, May 2012.
[18] A. Abdo, M. Sahin, D. S. Freedman, E. Cevik, P. S. Spuhler, and M. S. Unlu, "Floating light-activated microelectrical stimulators tested in the rat spinal cord," *J. Neural Eng.*, vol. 8, no. 5, Sep. 2011, Art. no. 056012.
[19] A. Kim, M. Ochoa, R. Rahimi, and B. Ziaie, "New and emerging energy sources for implantable wireless microdevices," *IEEE Access*, vol. 3, pp. 89–98, 2015.
[20] A. Cadei, A. Dionisi, E. Sardini, and M. Serpelloni, "Kinetic and thermal energy harvesters for implantable medical devices and biomedical autonomous sensors," *Meas. Sci. Technol.*, vol. 25, no. 1, Nov. 2013, Art. no. 012003.
[21] M. Dezyani, H. Ghafoorifard, S. Sheikhaei, and W. A. Serdijn, "A 60 mV input voltage, process tolerant start-up system for thermoelectric energy harvesting," *IEEE Trans. Circuits Syst. I, Reg. Papers*, vol. 65, no. 10, pp. 3568–3577, Oct. 2018.
[22] P. R. Troyk, "Injectable electronic identification, monitoring, and stimulation systems," *Annu. Rev. Biomed. Eng.*, vol. 1, no. 1, pp. 177–209, Aug. 1999.
[23] M. J. Kane, P. P. Breen, F. Quondamatteo, and G. ÓLaighin, "BION microstimulators: A case study in the engineering of an electronic implantable medical device," *Med. Eng. Phys.*, vol. 33, no. 1, pp. 7–16, Jan. 2011.
[24] X. Li, W. A. Serdijn, W. Zheng, Y. Tian, and B. Zhang, "The injectable neurostimulator: An emerging therapeutic device," *Trends Biotechnol.*, vol. 33, no. 7, pp. 388–394, Jul. 2015.
[25] L. Becerra-Fajardo, M. Schmidbauer, and A. Ivorra, "Demonstration of 2 mm thick microcontrolled injectable stimulators based on rectification of high frequency current bursts," *IEEE Trans. Neural Syst. Rehabil. Eng.*, vol. 25, no. 8, pp. 1343–1352, Aug. 2017.
[26] M. Seyedi, B. Kibret, D. T. H. Lai, and M. Faulkner, "A survey on intrabody communications for body area network applications," *IEEE Trans. Biomed. Eng.*, vol. 60, no. 8, pp. 2067–2079, Aug. 2013.
[27] S. A. Hackworth, "Design, optimization, and implementation of a volume conduction energy transfer platform for implantable devices," Ph.D. dissertation, Univ. Pittsburgh, Pittsburgh, PA, USA, 2010.

[28] W. Zhu, W. Fang, S. Zhan, Y. Zhou, Q. Gao, and X. Gao, "Volume conduction energy transfer for implantable devices," *J. Biomed. Res.*, vol. 27, no. 6, pp. 509–514, 2013.
[29] P. Chen, H. Yang, R. Luo, and B. Zhao, "A tissue-channel transcutaneous power transfer technique for implantable devices," *IEEE Trans. Power Electron.*, vol. 33, no. 11, pp. 9753–9761, Nov. 2018.
[30] A. M. Sodagar and P. Amiri, "Capacitive coupling for power and data telemetry to implantable biomedical microsystems," in *Proc. 4th Int. IEEE/EMBS Conf. Neural Eng.*, vol. 9, Apr. 2009, pp. 411–414.
[31] R. Jegadeesan, K. Agarwal, Y.-X. Guo, S.-C. Yen, and N. V. Thakor, "Wireless power delivery to flexible subcutaneous implants using capacitive coupling," *IEEE Trans. Microw. Theory Techn.*, vol. 65, no. 1, pp. 280–292, Jan. 2017.
[32] R. Erfani, F. Marefat, A. M. Sodagar, and P. Mohseni, "Modeling and experimental validation of a capacitive link for wireless power transfer to biomedical implants," *IEEE Trans. Circuits Syst. II, Exp. Briefs*, vol. 65, no. 7, pp. 923–927, Jul. 2018.
[33] J. S. Ho, "Wireless power transfer to deep-tissue microimplants," *Proc. Nat. Acad. Sci. USA*, vol. 111, no. 22, pp. 7974–7979, 2014.
[34] A. Ivorra, L. Becerra-Fajardo, and Q. Castellví, "*In vivo* demonstration of injectable microstimulators based on charge-balanced rectification of epidermically applied currents," *J. Neural Eng.*, vol. 12, no. 6, 2015, Art. no. 066010.
[35] J. P. Reilly, "Impedance and current distribution," in *Applied Bioelectricity: From Electrical Stimulation to Electropathology*. New York, NY, USA: Springer-Verlag, 1998, pp. 12–68.
[36] D. Andreuccetti, R. Fossi, and C. Petrucci, "An Internet resource for the calculation of the dielectric properties of body tissues in the frequency range 10 Hz-100 GHz," IFAC-CNR, Florence, Italy, Tech. Rep., 1997. [Online]. Available: http//niremf.ifac.cnr.it/tissprop/
[37] S. Grimnes and G. Martinsen, "Passive tissue electrical properties," in *Bioimpedance and Bioelectricity Basics*, 3rd ed. Amsterdam, The Netherlands: Elsevier, 2015, pp. 77–118.
[38] K. R. Foster and R. P. Schwan, "Dielectric properties of tissue," in *CRC Handbook of Biological Effects of Electromagnetic Fields*, C. Polk and E. Postow, Eds. Boca Raton, FL, USA: CRC Press, 1996, pp. 25–102.
[39] S. Grimnes and G. Martinsen, "Electrolytics," in *Bioimpedance and Bioelectricity Basics*, 3rd ed. Amsterdam, The Netherlands: Elsevier, 2015, pp. 9–36.
[40] A. Vander Vorst, A. Rosen, and Y. Kotsuka, *RF/Microwave Interaction With Biological Tissues*. Hoboken, NJ, USA: Wiley, 2006.
[41] *IEEE Standard for Safety Levels With Respect to Human Exposure to Radio Frequency Electromagnetic Fields, 3 kHz to 300 GHz*, Standard IEEE SCC39, The Institute of Electrical and Electronics Engineers, New York, NY, USA, 2005.
[42] International Commission on Non-Ionizing Radiation Protection, "Guidelines for limiting exposure to time-varying electric, magnetic, and electromagnetic fields (up to 300 GHz)," *Health Phys.*, vol. 74, no. 4, pp. 494–522, 1998.
[43] International Commission on Non-Ionizing Radiation Protection, "Guidelines for limiting exposure to time-varying electric and magnetic fields (1 Hz to 100 kHz)," *Health Phys.*, vol. 99, no. 6, pp. 818–836, 2010.
[44] S. R. Ward and R. L. Lieber, "Density and hydration of fresh and fixed human skeletal muscle," *J. Biomech.*, vol. 38, no. 11, pp. 2317–2320, Nov. 2005.
[45] D. J. Griffiths, "Special techniques," in *Introduction to Electrodynamics*, 3rd ed. Upper Saddle River, NJ, USA: Prentice-Hall, 1999, pp. 119–153.
[46] S. Grimnes and G. Martinsen, "Geometrical analysis," in *Bioimpedance and Bioelectricity Basics*, 3rd ed. Amsterdam, The Netherlands: Elsevier, 2015, pp. 141–178.
[47] T. Ohira, "Power efficiency and optimum load formulas on RF rectifiers featuring flow-angle equations," *IEICE Electron. Express*, vol. 10, no. 11, 2013, Art. no. 20130230.
[48] M. Tudela-Pi, L. Becerra-Fajardo, and A. Ivorra, "Powering implants by galvanic coupling: A validated analytical model predicts powers above 1 mW in injectable implants," in *World Congress on Medical Physics and Biomedical Engineering* (IFMBE Proceedings), vol. 68/3. Singapore: Springer, 2019.
[49] L. Becerra-Fajardo, R. Garcia-Arnau, and A. Ivorra, "Injectable stimulators based on rectification of high frequency current bursts: Power efficiency of 2 mm thick prototypes," in *Converging Clinical and Engineering Research on Neurorehabilitation II*. Cham, Switzerland: Springer, 2017, pp. 667–671.
[50] A. D. Dehennis, M. Mailand, D. Grice, S. Getzlaff, and A. E. Colvin, "A near-field-communication (NFC) enabled wireless fluorimeter for fully implantable biosensing applications," in *IEEE Int. Solid-State Circuits Conf. Dig. Tech. Papers*, Feb. 2013, pp. 298–299.
[51] K. Birmingham, V. Gradinaru, P. Anikeeva, W. M. Grill, V. Pikov, B. McLaughlin, P. Pasricha, D. Weber, K. Ludwig, and K. Famm, "Bioelectronic medicines: A research roadmap," *Nature Rev. Drug Discovery*, vol. 13, no. 6, pp. 399–400, May 2014.
[52] X. Navarro, T. B. Krueger, N. Lago, S. Micera, T. Stieglitz, and P. Dario, "A critical review of interfaces with the peripheral nervous system for the control of neuroprostheses and hybrid bionic systems," *J. Peripheral Nervous Syst.*, vol. 10, no. 3, pp. 229–258, Sep. 2005.
[53] J. Andreu-Perez, D. R. Leff, H. M. D. Ip, and G.-Z. Yang, "From wearable sensors to smart implants-toward pervasive and personalized healthcare," *IEEE Trans. Biomed. Eng.*, vol. 62, no. 12, pp. 2750–2762, Dec. 2015.

MARC TUDELA-PI was born in Vilanova de Bellpuig, Spain, in 1990. He received the M.Sc. degree in industrial electronic engineering from the Universitat Politècnica de Catalunya, in 2013, and the M.Sc. degree in biomedical engineering from the Universitat de Barcelona, and the Universitat Politècnica de Catalunya, in 2019. He is currently pursuing the Ph.D. degree with Universitat Pompeu Fabra, Barcelona, Spain.

He worked as a Control Engineer at the private sector designed high-power electronic converters, from 2013 to 2017. Since September 2017, he has been with the Biomedical Electronics Research Group (BERG), Universitat Pompeu Fabra. His research interests include wireless power transfer for medical implants, bioelectronics, and bioimpedance.

LAURA BECERRA-FAJARDO received the B.Sc. degree in electronic engineering from the Universidad Nacional de Colombia, in 2008, the M.Sc. degree in biomedical engineering from the Universitat de Barcelona and the Universitat Politècnica de Catalunya, in 2012, and the Ph.D. degree from Universitat Pompeu Fabra (UPF), Barcelona, in 2016.

After working as a Research Engineer with the Translational Research and Knowledge Management Team (Research and Development), Otto Bock GmbH, Duderstadt, Germany, she became a Postdoctoral Fellow at UPF. Her research focuses mainly in exploring and designing miniaturized medical devices for sensing and electrical stimulation.

ARACELYS GARCíA-MORENO was born in Caracas, Venezuela, in 1982. She received the B.Sc. degree in electronic engineering from Universidad Simon Bolivar, Caracas, in 2005, and the M.Sc. degree in biomedical engineering from Ghent University, Ghent, Belgium, and RWTH Aachen University, Aachen, Germany, in 2017. She is currently pursuing the Ph.D. degree with the Department of Information and Communication Technologies, Universitat Pompeu Fabra, Barcelona, Spain.

Since October 2017, she has been a Predoctoral Trainee Researcher. Her research focuses on the design, optimization and implementation of processes, and techniques and components for the construction of implantable electronic devices for electrical stimulation.

JESUS MINGUILLON was born in Granada, Spain, in 1990. He received the M.Sc. degree in telecommunication engineering, the M.Sc. degree in electrical and electronic engineering, and the Ph.D. degree in information and communication technologies from the University of Granada, Granada, Spain, in 2014, 2015, and 2018, respectively.

He worked on the design and development of non-invasive brain–computer interfaces and other biosignal-based systems. Moreover, he investigated the use of these systems in daily-life contexts and published his main results in international high-impact journals and conferences. He is currently a Postdoctoral Researcher with the Biomedical Electronics Research Group (BERG), Pompeu Fabra University, Barcelona, Spain. His main research focuses on the design and development of power supply and bidirectional communication systems (hardware–software) for volume-conduction-based implants, in the framework of two European projects: Electronic AXONs (wireless microstimulators based on electronic rectification of epidermically applied currents) and EXTEND (Bidirectional Hyper-Connected Neural Systems).

ANTONI IVORRA received the Ph.D. degree in electronics engineering from the Universitat Politècnica de Catalunya, Barcelona, Spain, in 2005. He is currently an Associate Professor with Universitat Pompeu Fabra (UPF), Barcelona, where he leads the Biomedical Electronics Research Group. Prior to joining the UPF, in 2010, he enjoyed a four-year postdoctoral stay at the University of California at Berkeley, from 2005 to 2009, followed by an eight-month Postdoctoral position at the CNRS-Institut Gustave Roussy, Villejuif, France. From 1998 to 2005, he was with the Biomedical Applications Group, Centre Nacional de Microelectrònica, Bellaterra, Spain. He is the author or coauthor of 50 publications in peer-reviewed journals, four book chapters, and more than 35 conference contributions. He is the inventor or co-inventor of 11 families of patent applications. His research is focused on bioelectrical phenomena and, in particular, on exploring the use of these phenomena for implementing new methods and devices for biomedical applications. Specifically, his main research topics are electroporation, particularly for tissue ablation, electrical bioimpedance for diagnostic purposes, and injectable electronics for neuroprosthetics.